RECEIVED
JAN 11 1995
OSTI

A 10-GeV, 5-MW PROTON SOURCE FOR A PULSED SPALLATION SOURCE* +

Y. Cho, Y.-C. Chae, E. Crosbie, H. Friedsam, K. Harkay, D. Horan, R. Kustom,
E. Lessner, W. McDowell, D. McGhee, H. Moe, R. Nielsen, G. Norek, K. J. Peterson,
K. Primdahl, Y. L. Qian, K. Thompson, and M. White

Argonne National Laboratory, Argonne, IL 60439, USA

ABSTRACT

A feasibility study for a pulsed spallation source based on a 5-MW, 10-GeV rapid cycling proton synchrotron (RCS) is in progress. The integrated concept and performance parameters of the facility are discussed. The 10-GeV synchrotron uses as its injector the 2-GeV accelerator system of a 1-MW source described elsewhere [1-7]. The 1-MW source accelerator system consists of a 400-MeV H⁻ linac with 2.5 MeV energy spread in the 75% chopped (25% removed) beam, and a 30-Hz RCS that accelerates the 400-MeV beam to 2 GeV. The time-averaged current of the accelerator system is 0.5 mA, equivalent to 1.04×10^{14} protons per pulse. The 10-GeV RCS accepts the 2 GeV beam and accelerates it to 10 GeV. Beam transfer from the 2-GeV synchrotron to the 10-GeV machine utilizes highly efficient bunch-to-bucket injection, so that the transfer can be made without beam loss. The synchrotron lattice uses FODO cells of 90° phase advance. Dispersion-free straight sections are obtained using a missing magnet scheme. The synchrotron magnets are powered by dual-frequency resonant circuits. The magnets are excited at a 20-Hz rate and de-excited at 60-Hz, resulting in an effective 30-Hz rate. A key feature of the design of this accelerator system is that beam losses are minimized from injection to extraction, reducing activation to levels consistent with hands-on maintenance. Details of the study are presented.

I.   Introduction

Proton beam power in the MW range with a pulse repetition rate of 30 to 60 Hz can be attained by several accelerator configurations; they can be divided into two basic categories.

In one category, a full-energy pulsed linear accelerator (linac) and pulse compressor ring or rings are used. A typical linac pulse length is of the order of 1 msec, and the compressor ring shortens the beam pulse length to the desired microsecond range. In general, a higher energy linac is expensive to construct and to operate. This is one reason that the highest energy proton linac built to date has less than 1-GeV energy. If the linac energy is chosen in a range around 1 GeV, a 5-mA beam current is required to obtain 5 MW of beam power. This is the low-energy, high-current option.

In the other category, a low energy linac injects beam into a circular accelerator that provides most of the proton energy as a result of multiple revolutions around the ring. This combination of a low energy linac and a synchrotron to obtain high proton beam energy has been standard technology for decades. A typical synchrotron energy gain is about a factor of 10, thus the injector linac energy can be a factor of ten less than the final beam energy. If the final synchrotron energy is chosen to be 10 GeV, a beam current of 0.5 mA is required to produce 5 MW of beam power. This is the high-energy low-current option. A disadvantage of this method is that a synchrotron can accelerate a limited amount of beam. The most recent record for the number of protons accelerated per pulse is 6.3×10^{13}, set by the AGS at BNL. The 1×10^{14} protons/pulse requirement for 0.5 mA current at 30 Hz can be reached with appropriate R&D and design features.

One of the most important design considerations is the prevention of beam losses during all phases of transport and acceleration. Handling a smaller number of particles (lower current) should result in lower losses. Past experience has shown that the most likely time for beam losses to occur is during multi-turn injection into a ring. If there are injection losses, it is best that they occur at low energy to minimize activation. For these reasons, we propose to have the highest possible proton energy and lowest possible beam current for this source.

This study of a 10-GeV, 5-MW proton source is an extension of a feasibility study of a 1-MW 2-GeV 30-Hz pulsed neutron source to upgrade the ANL Intense Pulsed Neutron Source (IPNS) [1]. The harmonic number in the 2-GeV machine was increased from one to two in this 5-MW study. The 10-GeV synchrotron accepts the 2-GeV (0.5-mA) beam from the 1-MW source and accelerates it to 10 GeV. Beam transfer from the 2-GeV RCS (RCS-I) to the 10-GeV RCS (RCS-II) is performed using bunch-to-bucket transfer. A detailed study of this transfer showed that no-loss injection can be achieved.

The 1-MW facility design takes into account existing infrastructure in the former ZGS (12-GeV Zero Gradient Synchrotron) buildings, totaling about 50,000 m^2 of space. The accelerator configuration for the 1-MW facility consists of a 400-MeV injector linac and a 400-MeV to 2-GeV synchrotron. The 10-GeV accelerator system is housed in a new enclosure adjacent to the ZGS complex.

Geometric layouts of the 1-MW and 5-MW facilities are arranged such that construction of the 5-MW system does not interfere with operation of the 1-MW source except during the last minute link-up between the two accelerator systems. This geometric separation between the two accelerators enables the 5-MW facility to be constructed in stages without interfering with operations, and utilizes all previous investments. Figure 1 shows the layout of the proposed facility and clearly indicates the 5-MW addition.

II. Lattice

The required features of the 10-GeV lattice are similar to those of the 2-GeV lattice: 1) the transition energy must be larger than the extraction energy so that the lattice has a relatively large slip factor, $\eta = \left| \gamma^{-2} - \gamma_t^{-2} \right|$, 2) there must be enough straight-section length for the radio-frequency cavity system that could have a total length of ≈ 200 m, and 3) the straight sections should be dispersion-free so that the rf cavities can be placed in dispersion-free regions. In addition, the circumference of the 10-GeV ring should be a multiple of that of the 2-GeV ring

in order to have a harmonic relationship between the two synchrotron rf systems during bunch transfer from one machine to the other.

One way to satisfy requirement 1) above is for the lattice to have a large horizontal tune, since the transition energy, γ_t, is proportional to the horizontal tune. A FODO cell lattice with a phase advance of approximately 90° in both transverse planes was chosen for the normal cell in order to obtain a higher tune.

Additional advantages of the 90° FODO cells are: 1) Dispersion suppression can be obtained by removing a dipole from a normal cell. 2) Normal cells without both dipoles can be used to construct the straight-section cells. 3) Focusing quadrupoles in the normal cells, the dispersion-suppressor-cells and the straight-section cells have the same strength, and therefore only one power supply is needed for the quadrupole family. Similarly, defocusing quadrupoles in the ring can also be powered by a single power supply.
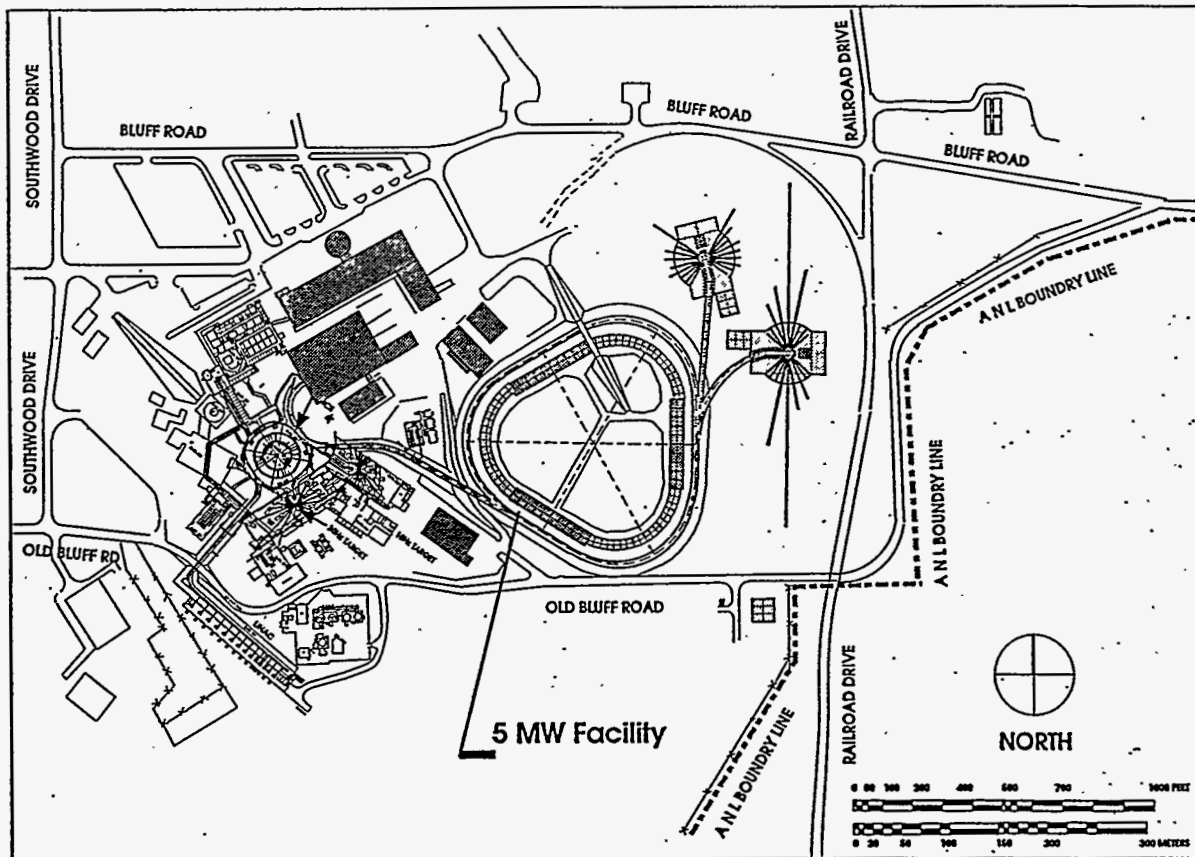
Figure 1: Site Layout Showing the Location of the 5-MW Facility.

Figure 2 shows 1/2 of a super period with reflective symmetry at both ends. Each cell of the FODO structure has a phase advance of ~ 90° in both transverse planes. The normal cells, dispersion-suppressor cell and the straight-section cells are evident in the figure. Dispersion suppression is achieved by removing a dipole from a normal cell. The missing dipole scheme suppresses the dispersion function when the vertical phase advance is slightly less than 90° while maintaining a horizontal phase advance of 90°. A benefit of this arrangement is that the horizontal tune is about one unit higher than the vertical tune, which is a good feature. Further study of this lattice showed that the lattice tunes can be adjusted to within ± 1/2 unit while

maintaining the tune difference of one unit and a vanishing dispersion function through the straight sections.

The circumference ratio between the 10-GeV ring and the 2-GeV ring is four, giving RCS-II a circumference of 7.61.6 m. The superperiodicity of the 10-GeV ring was chosen to be three, so that the ring fits into the available space and reduces the required number of dispersion-suppressor cells. Table 1 shows the normal cell parameters. The overall lattice parameters are shown in Table 2.

Table 1: Normal Cell Parameters for RCS-II
(10 GeV, B ρ = 36.352 T·m, Cell Length 10.155 m)

Elements	Length (m)	Strength	Units
QD	0.4	-13.086	T/m
DQS	0.2		
SD	0.4	-1.299	m^{-2}
DSB	0.675		
B	1.72735	1.377	T
DBQ	1.275		
QF	0.8	13.536	T/m
DQS	0.2		
SF	0.4	0.867	m^{-2}
DSB	0.675		
B	1.72735	1.377	T
DBQ	1.275		
QD	0.4	-13.086	T/m

III. Apertures

The 2-GeV beam from RCS-I has a transverse emittance of 128 π mm mr. The beam-stay-clear (BSC) acceptance of the 10-GeV ring is defined by twice the emittance and $\pm$ 1 % of the momentum spread of the incoming beam. This method is similar to that used in the 2-GeV ring. Figure 3 shows a vacuum chamber cross-section at a focusing quadruple indicating the BSC and the injected beam envelope in RCS-II.

IV. Dynamic Aperture

The natural tune of the 90° FODO lattice is 18.75 in both transverse planes. The working point must be chosen taking a large tune spread due to space charge into account, since the lattice has to provide a large enough dynamic aperture to contain the beam. The space charge effects are greatest during the low energy injection, where the maximum tune shift was estimated to be about 0.18 in each plane. In addition to the space-charge induced tune spread, there is a tune spread due to the momentum spread. If we assume a beam with $\Delta p/p$ = 1%, the chromatic tune spread is larger than the space-charge tune spread. Thus chromaticity correction is necessary, especially during injection.

In order to find the optimum working point, the tune region where the dynamic apertures are largest was searched. As a result of extensive tracking studies, the optimal tune range was found to be $19 < \nu_x < 19.25$ and $18 < \nu_y < 18.25$ to provide enough dynamic aperture to contain the beam at injection. We chose the lattice tunes to be $\nu_x = 19.20$ and $\nu_y = 18.19$. The
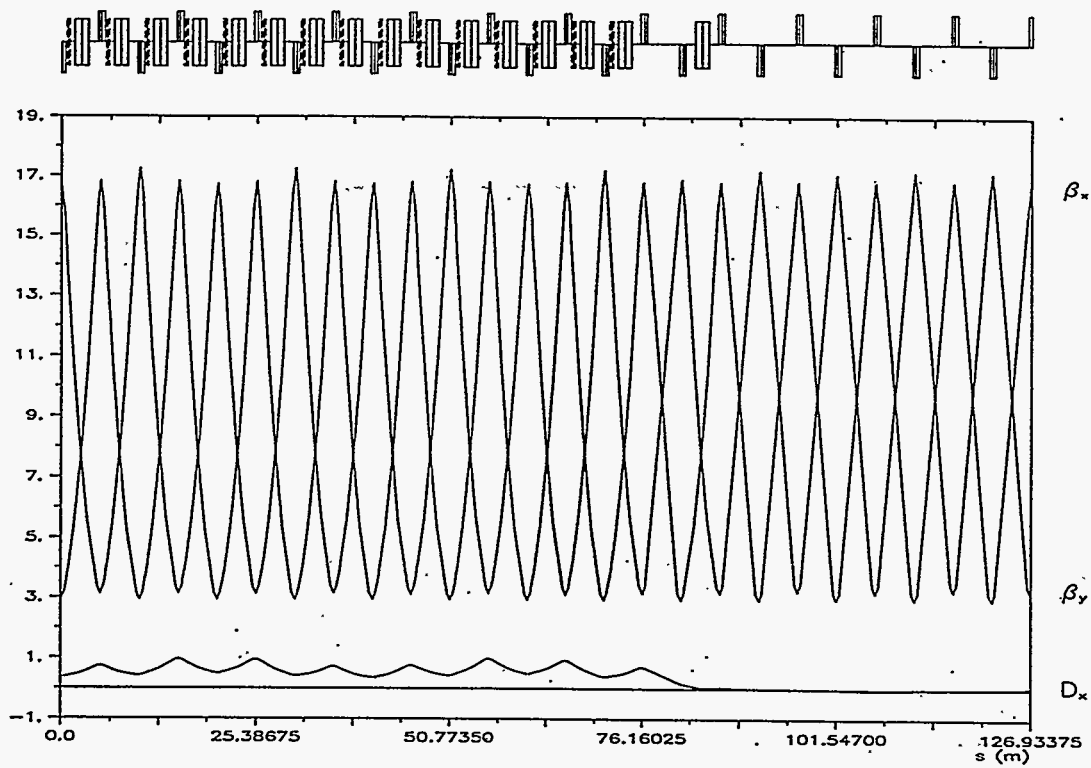
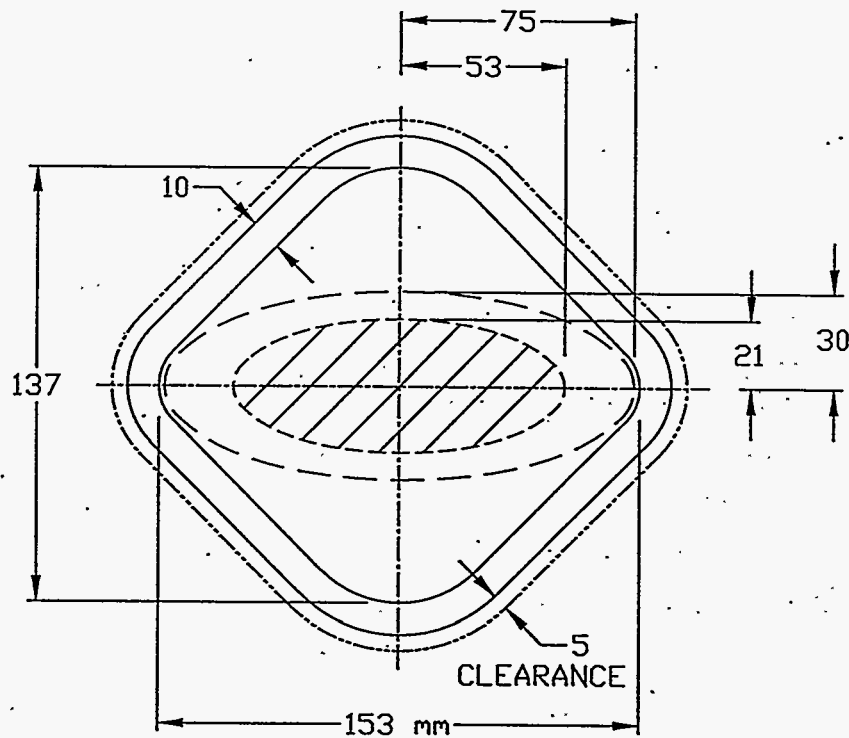**Figure 2:** Lattice Functions for 1/2 Super-Period.

Figure 3: Focusing Quadrupole Vacuum Chamber Cross Section Showing Beam-Stay-Clear (dashed line) and Beam Envelope (area containing diagonal lines).

working point, including the space-charge tune spread, is clear of structure resonances and is shown in the tune diagram in Figure 4.

The lattice dynamic apertures at the design tune and at the depressed tune are shown in Figure 5. The beam size at injection and the BSC are also shown. In Figure 5(a), we show the dynamic apertures at the chromaticities $\xi_{x,y} = 0$ and -5. The operating range of the chromaticity is expected to be close to $\xi_{x,y} = -5$, where the dynamic aperture is shown to be larger than the BSC. In Figure 5(b), we show the dynamic aperture when the lattice is adjusted to the space-charge depressed tune.
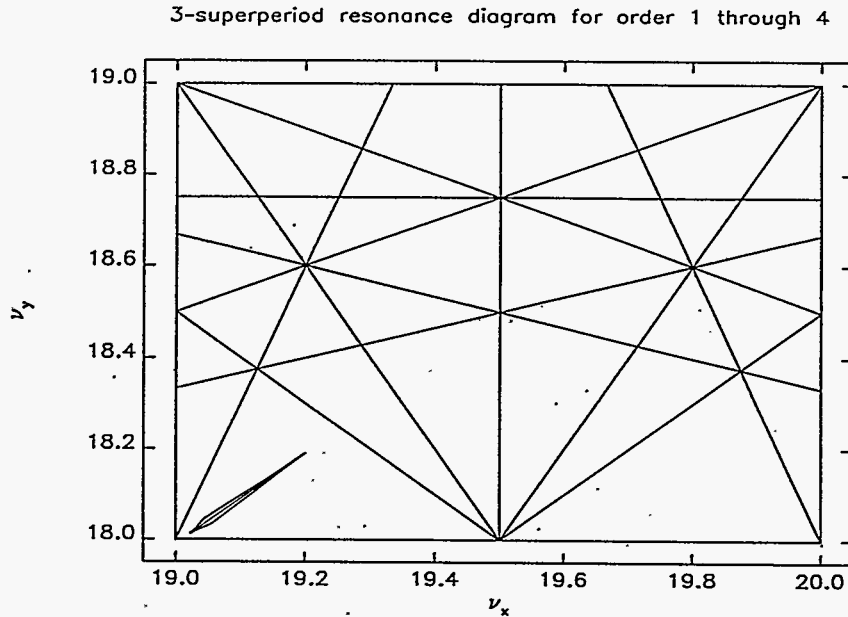
3-superperiod resonance diagram for order 1 through 4

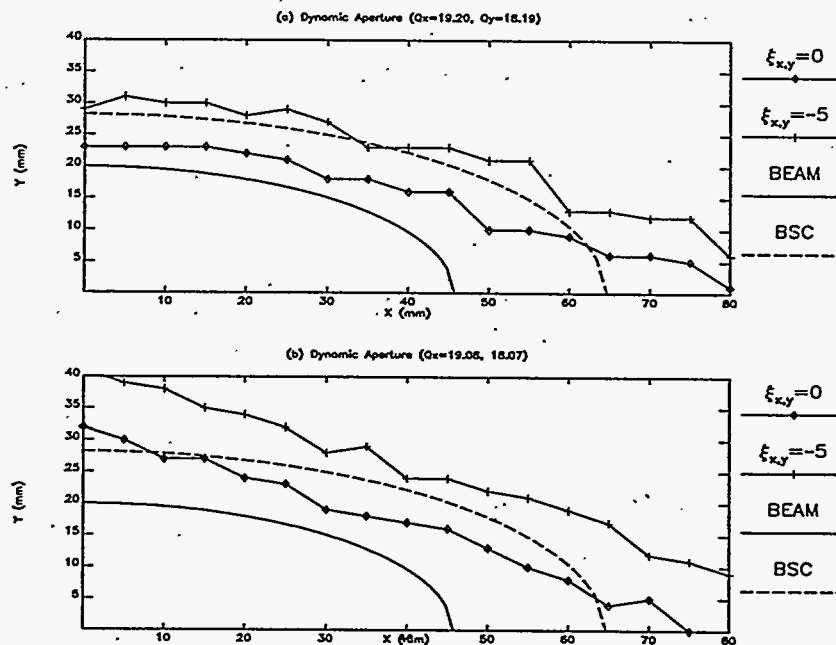**Figure 4:** 1st through 4th Order Resonance Diagram Including Working Point and Tune Spread.

Figure 5: Dynamic Aperture of the Lattice at Different Chromaticities. (a) Lattice at the Design Tune $v_x = 19.20$ and $v_y = 18.19$. (b) Lattice at the Depressed Tune $v_x = 19.08$ and $v_y = 18.07$, Where a Uniform Charge Distribution is Assumed.

Since the particle at the edge of the beam is oscillating with large amplitude at this tune, the dynamic aperture is critical. This consideration is already taken into account in choosing the working point, resulting in the large aperture at the depressed tune, shown in Figure 5(b).

Table 2: Lattice Parameters for RCS-II.
(10 GeV, B $\rho = 36.352$ T·m)

Parameters	Value	Units
Circumference	761.6	m
Superperiodicity	3	
Total Number of Cells	75	
Number of Normal Cells	45	
Number of Dispersion-suppressor Cells	6	
Number of Straight-section Cells	24	
Nominal Length of Cell	10.155	m
Nominal Length of Straight Section	4.277	m
Bending Radius	26.392	m
Number of Dipole Magnets	96	
Dipole Magnets Effective Length	1.72735	m
Dipole Field Strength at Extraction (10 GeV)	1.377	T
Dipole Field Strength at Injection (2 GeV)	0.352	T
Number of Quadrupole Magnets	150	
Quadrupole Magnet Effective Length	0.8	m
Maximum Quadrupole Gradient (B')	13.54	T/m
Number of Sextupole Magnets (F)	42	
Number of Sextupole Magnets (D)	48	
Sextupole Magnet Effective Length	0.4	m
Sextupole Field Coefficient (B'')	118.1	T/m^2
Transition Energy γ_t	14.83	
Horizontal Tune, ν_x	19.20	
Vertical Tune, ν_y	18.19	
Natural Chromaticity, $\xi_x = (\Delta\nu)_x/(\Delta p/p)$	−23.90	
Natural Chromaticity, $\xi_y = (\Delta\nu)_y/(\Delta p/p)$	−23.06	
Maximum β_x	16.84	m
Maximum β_y	17.26	m
Maximum Dispersion Function	1.0	m

V. Injection

Each pulse of the 2-GeV extracted beam from RCS-I contains two bunches separated by 332 nsec. Each bunch contains 5×10^{13} protons, and has an area of 3.7 eV·sec. The rf frequency of RCS-I at extraction is 3 MHz, with a harmonic number of 2.

The two bunches from each RCS-I pulse are transferred into waiting RCS-II buckets. Two RCS-I bunches at 3 MHz are injected into two buckets of the 6-MHz RCS-II rf system. As a consequence of this change in the rf frequency and the ratio of circumferences of the machines, RCS-II has 16 buckets (harmonic number = 16) of which only two are occupied by the beam, separated by an empty bucket.

VI. Rf Voltage Program

The key feature of the design studies for both the 1- and 5-MW machines was to determine the rf programming such that there is no beam loss from injection to extraction. Such programming was obtained using a Monte Carlo method to track the particles from injection to extraction [8].

VI.1 Rf Voltage at Injection:

The 2-GeV beam from RCS-I has a single bunch area of 3.7 eV sec; this bunch is injected into a slightly larger waiting bucket in RCS-II. Matching between the bunch and the bucket is performed using the following algorithm. The rf voltage at the extraction of the 2-GeV beam determines the energy spread, ΔE, and length, Δt, of the bunch. The energy spread and bunch length of the incoming beam are matched to a phase space contour of the waiting bucket. The space charge suppression of the phase space area is taken into account in these considerations to prevent mismatching and consequent dilution of the beam. Figure 6(a) shows the rf bucket and the bunch population in RCS-I at extraction. Figure 6(b) shows the bunch injected into the waiting bucket of RCS-II. The dashed line in Figure 6(b) represents the Hamiltonian contour whose height, ΔE, and whose enclosed area are equal to those of the injected beam. This shows that the 3.7 eV sec bunch is matched to a contour of a 3.7 eV sec phase space area within a 5.8 eV sec bucket. The required rf voltage at this time is 0.7 MV.

VI.2 Rf Voltage Program During Acceleration:

The rf voltage program for the accelerating cycle is depicted in Figure 7(a). The time variation of the bucket and bunch area is shown in Figure 7(b).

During the first eight msec of acceleration the rf voltage is raised to maintain the 5.8 eV sec bucket area determined by the previously described procedure. The rf voltage increases from 0.7 MV to 1.9 MV, and reaches a maximum at 8 msec. From this time to the end of acceleration, the voltage is decreased gradually from 1.9 MV to 1.7 MV. The bucket area grows from 5.8 eV sec to 106.3 eV sec. The voltage for the latter part of the cycle is maintained high to ensure a synchrotron frequency fast enough to allow the particles in the bunch to follow the rapid change of the synchronous phase near extraction. The bunch area is 3.7 eV sec throughout the cycle. At extraction, the bunch height is ±102.5 MeV and the bunch length is ±11.3 nsec. The final bunch length can be tailored to a longer or shorter length by rf manipulations, as is explained in detail in the following subsection.

The rf voltage program is able to capture and accelerate 1×10^{14} particles per pulse with no loss of particles during the beam transfer and acceleration processes.

VI.3 Rf Voltage Manipulation to Adjust the Bunch Length:

The RCS-II bunch length at extraction can be tailored to the specific application through rf manipulations. The typical full bunch length at extraction without any manipulations is between 22 and 25 nsec. The bunches can be shortened through bunch rotation prior to extraction. Using a combination of bunch rotation and debunching, the bunches can be lengthened. An overlap of the two bunches can be achieved in about 3.5 msec, if there is a flat-top in the ring magnetic field.
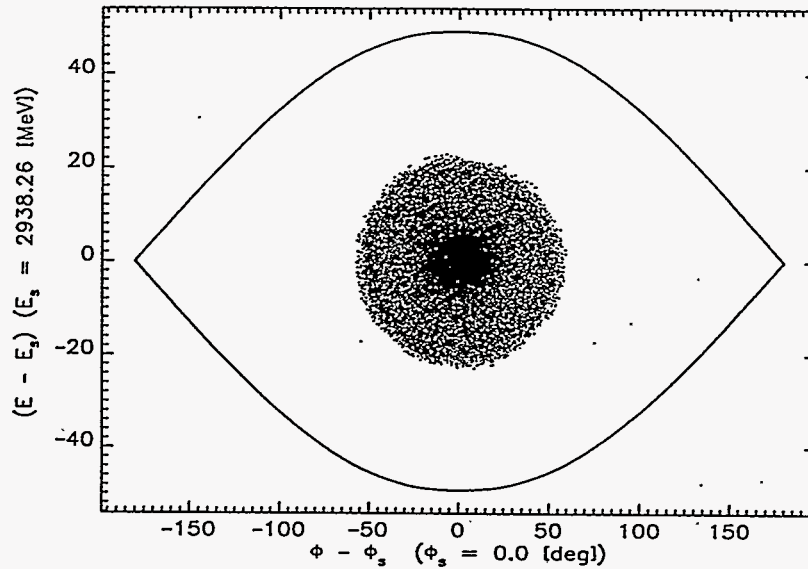

Figure 6(a): Rf Bucket and Phase Space Distribution at Extraction in RCS-I.
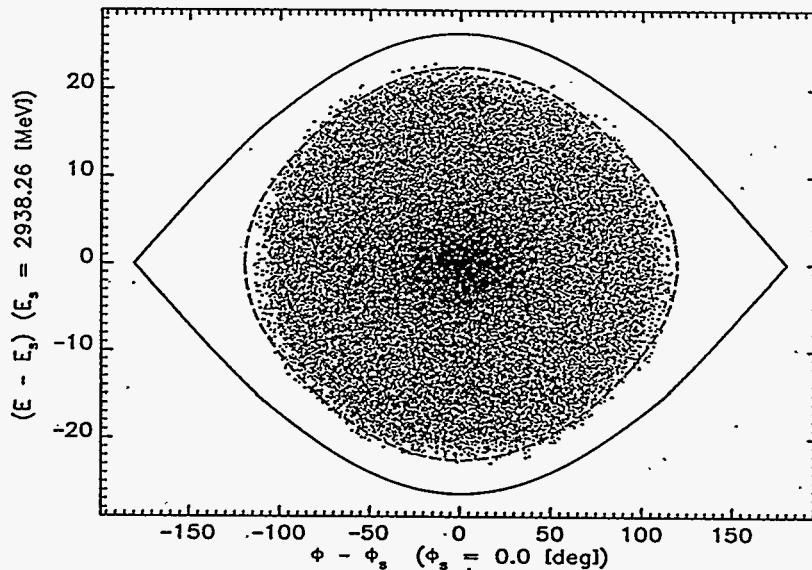

Figure 6(b): Rf Bucket and Phase Space Distribution at Injection in the RCS-II. The Dotted Line Indicates the Contour Enclosing an Area of 3.7 eV sec.
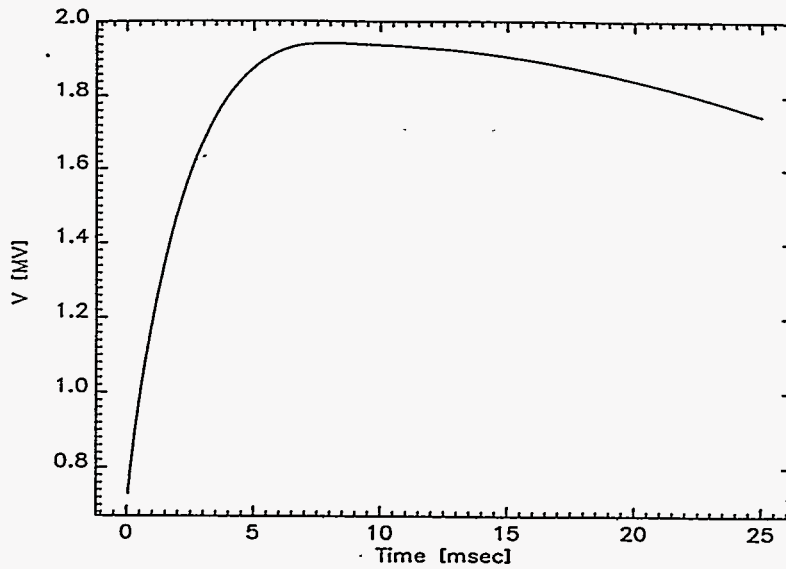
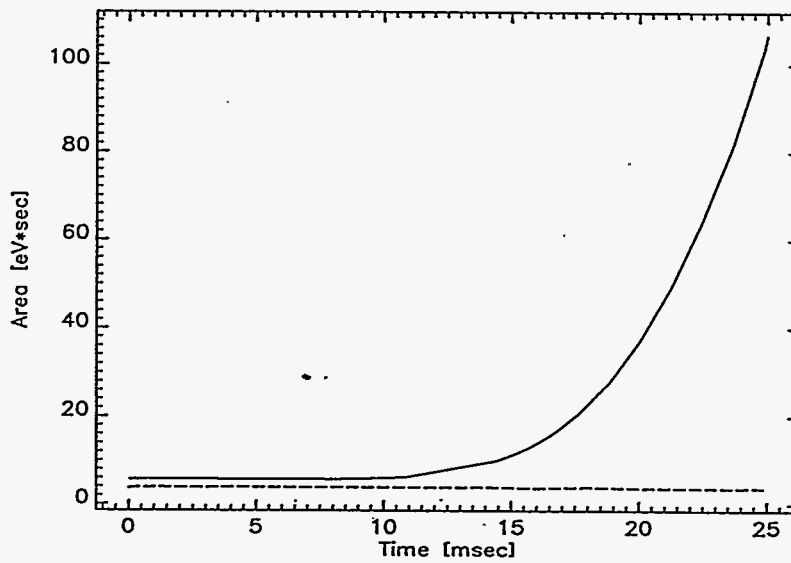**Figure 7(a):** Rf Voltage Program for the Acceleration Cycle.

Figure 7(b): Time Evolution of the Bucket (solid line) and Bunch (dotted line) Areas During the Acceleration Cycle.

For bunch rotation to shorten the bunch, the voltage step, V_1, is related to the final, desired half-bunch length in radians, ϕ_1, and initial energy spread, ΔE_0, through

$$V_1 = \frac{\pi h |\eta|}{2\beta^2 E_s} \frac{\Delta E_0^2}{e \sin^2(\phi_1/2)}.$$

Longitudinal particle tracking results using several rf voltage steps and two initial bunch lengths agree well with this relationship. In the tracking study, the voltage is increased in 50 μsec. The voltage V_1 can be minimized by starting with a long bunch. When the bunch length at the start of rotation is 25 nsec and the $\Delta p/p$ is 0.9% ($V_{rf} = 1.25$ MV), a voltage $V_1 = 3.2$ MV results in a bunch length of 15 nsec and $\Delta p/p$ of 1.5% after 0.45 msec (1/4 synchrotron period). The phase space distribution of the bunch at the end of rotation from the Monte Carlo studies is shown in Figure 8(a). Note that the bunch length has changed from 25 nsec to 15 nsec.

A combination of bunch rotation and debunching can be used to increase the bunch length. The rf voltage is set to zero at the end of the ramp, with or without first rotating the bunch, and the beam is allowed to drift on a flat-top. The new full bunch length, τ_1, is related to the drift time, t, and the full bunch length at the beginning of the drift, τ_0, through

$$\tau_1 = 2|\eta|\frac{\Delta p}{p}t + \tau_0,$$

where τ_1 and τ_0 have units of time. Without first rotating the bunch and starting with $\Delta p/p = 0.9\%$ ($\tau_0 = 25$ nsec), the bunch length increases by about 50 nsec for every 1 msec of drift. After rotating the bunch to $\Delta p/p = 1.5\%$ ($\tau_0 = 15$ nsec), the bunch length increases by about 90 nsec for every 1 msec of drift. The resulting phase space distribution after 1.5 msec drift from Monte Carlo studies is shown in Figure 8(b). At extraction, the rf frequency is 6.3 MHz; therefore, the bunches are separated by 320 nsec. Complete decoherence, or just overlapping of both bunches, can be achieved in the latter example after about 3.5 msec of drift. This results in a single bunch with length ≥ 640 nsec.

VII. Impedance and Collective Instabilities

Longitudinal and transverse instability thresholds were obtained after the coupling impedances were estimated. The transverse impedance is dominated by space charge. The contribution to the longitudinal impedance from space charge is comparable to that from the broadband rf cavity impedance. Beam parameters such as $\Delta p/p$ and peak current were obtained through Monte Carlo studies of beam capture and acceleration using a longitudinal tracking code that includes the effects of space charge [8]. The analysis lead to an rf voltage profile and beam parameters that minimize the instabilities as well as beam losses.

RCS-II operates below the transition energy, thus the longitudinal microwave instability is not expected to occur unless there is a large resistive component. However, a conservative approach was adopted to ensure that the momentum spread is sufficient to satisfy the Keil-Schnell (KS) stability criterion. The space charge impedance is smaller in RCS-II than in RCS-I by a factor of between 5 and 10. Therefore, a contour-following rf shield, such as that used in the RCS-I and ISIS [9], is not required. The vacuum chamber is constructed of ceramic with a fixed-position wire rf shield. The KS criterion is difficult to satisfy in RCS-II because the threshold is dominated by the high peak current and a small slip factor. Studies were performed to choose an rf voltage profile that provides adequate bucket area and momentum spread. Tracking studies show that the beam remains in the stable region through most of the acceleration, where, at extraction energy, the $\Delta p/p$ is about 1% and the bunching factor (peak/circulating current) is about 0.01. The peak current is 160 A at injection and < 800 A at extraction.

In the transverse plane, the head-tail instability was analyzed. The growth rate is proportional to the resistive wall and kicker impedance. With a chromaticity corrected to zero and estimating the kicker impedance to be < 60 kΩ/m, the fastest growth rate is < 120 sec^{-1}. The head-tail modes are stabilized at a slightly negative chromaticity. The threshold tune spread for transverse microwave instability is 0.11. Given a $\Delta p/p$ of 1%, stability is satisfied by a chromaticity $\xi \leq -1$.
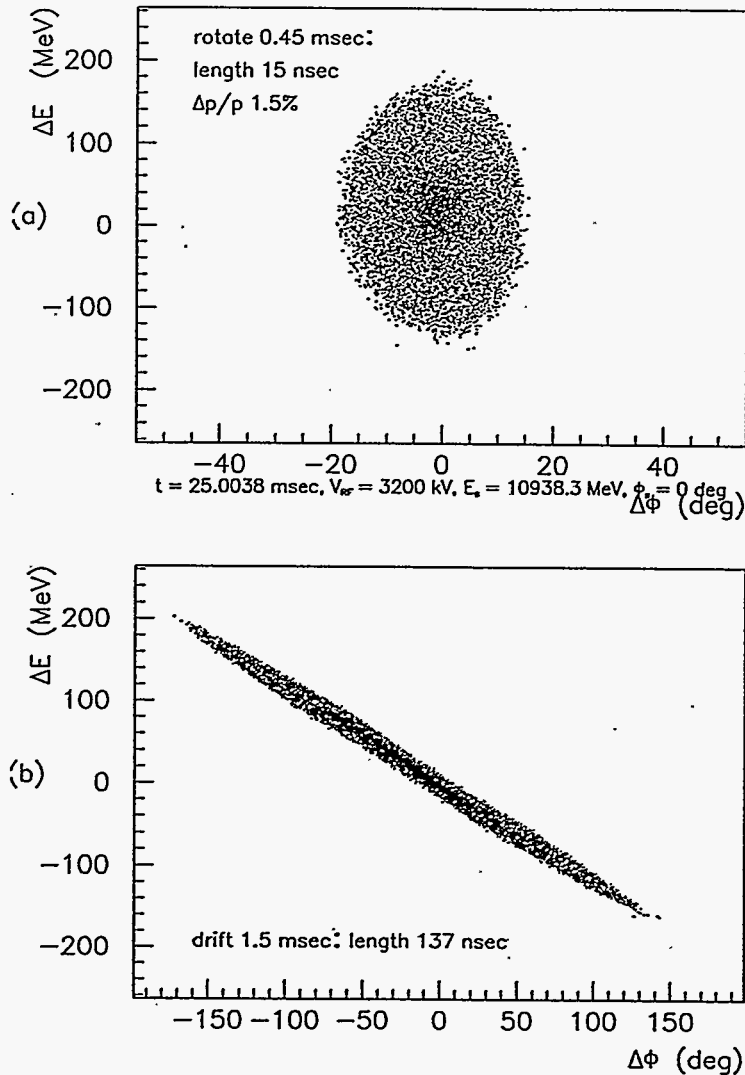

Figure 8: Effect of Rf Manipulations on Bunch: (a) Bunch Rotation with Rf Voltage of 3.2 MV and (b) Debunching with Zero Rf Voltage.

VIII. Synchrotron Hardware

The following is a short summary of the RCS-II hardware systems.

VIII.1 Synchrotron Magnets

The dipole, quadrupole and sextupole magnets for the synchrotron are designed for nominal beam energies of 10 GeV but are capable of handling a maximum value of 11 GeV. The gap geometries were scaled down from the corresponding magnets in the RCS-I ring to fit the smaller vacuum chambers. Calculated field qualities for the RCS-II magnets are, therefore, nearly identical to the RCS-I values.

Some of the major parameters for each of the synchrotron ring magnets are listed in Table 3. The rms currents listed there are based on a simple 30-Hz biased excitation, and not on the dual-frequency excitation described in Section VIII.2. An end-view of a quadrupole is shown in Figure 9.
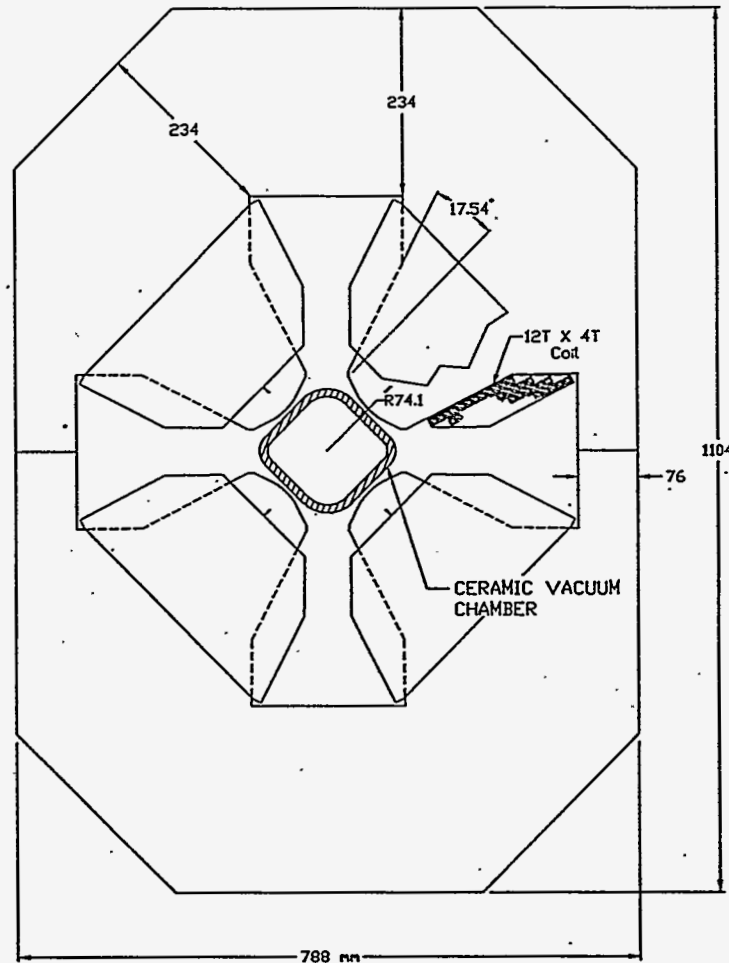

Figure 9: End View of a Synchrotron Quadrupole Magnet.

The cores of these magnets are parallel stacks of low-silicon steel laminations that are 0.36-mm thick. Each consists of 2 or 3 sections, allowing it to be assembled around the vacuum chamber. Bonded end-packs at the ends of each section contain the special contouring required to control field shapes at the ends. Each core section is held under compression by welded tie-bars and insulated tie-rods. The pole taper-angles keep the flux densities on the pole axes below saturation, and the average flux densities in the yokes are between 1.0 and 1.2 T.

The coils for these magnets contain hollow copper conductor that is insulated with polyimide film, fiberglass tape, mica tape and vacuum-impregnated, heat-cured epoxy. Although the insulating materials are radiation resistant, radiation exposures of the coils are further reduced by locating them well away from the midplanes. Parallel electrical paths are used to allow the use of smaller conductors to control eddy current losses and to keep the peak voltages across a series-connected group of magnets at manageable levels. The parallel circuits extend around pairs of poles for a given magnet so as to equalize the impedances of all paths. Magnet cooling is provided by deionized water with a maximum supply temperature of 32°C and a pressure gradient of 6.9 bars across all magnets.

Table 3: Parameters for the Synchrotron Ring Magnets

Parameters		Dipole	Quadrupole	Sextupole	Units
Number Required		90	150	90	
Peak Strength at 10.0 GeV		1.38 T	13.54 T/m	118.1 T/m^2	
Effective Length		1.73	0.8	0.40	m
Gap Height or Diameter		131.4	148.2	166.6	mm
Total Mass of Magnet		16000	3750	720	kg
Conductor	Height	8.9	8.9	7.3	mm
	Width	8.9	8.9	7.3	mm
	Hole Diameter	4.9	5.3	4.1	mm
Number Turns per Pole		10	8	16	
Number of Parallel		40	6	2	
Total Inductance		2.5	1.8	7.8	mH
Total Resistance		0.74	3.5	21	mW
Supply Current	Max.	7264	3877	590	A
	Min.	1856	991	151	A
	rms	4945	2639	402	A
Power Losses		32.3	28.0	3.6	kW
Total Water Flow		1.13	0.77	0.19	l/sec
Water Temp. Rise		7	9	5	°C

VIII.2 Power Supplies

The RCS ring magnets are energized with dual-frequency resonant power supplies, that excite the ring at a 20-Hz rate and de-energize it at a 60-Hz rate. This method, similar to that proposed in the 1-MW source [1,7] results in an overall repetition rate of 30 Hz, and reduces the peak rf voltage required for acceleration by one third.

VIII.3 Vacuum Chamber System

The vacuum chambers through the RCS ring magnets are 99.7% pure alumina ceramic similar to those used in RCS-I [1,7]. There are rf shields close to the inside surface of each chamber section. Figure 3 shows a cross section of the chambers in the quadrupole and sextupole magnets.

VIII.4 Radio-Frequency System

The design of the cavities for the 10-GeV ring uses type 4M2 ferrite, the same ferrite used on the ISIS RCS [10] and for which extensive measurements were made at BNL [11]. Each cavity is built in a double-cell configuration similar to the ISIS cavities. The physical length of the full cavity from flange-to-flange is 3.46 m. A ground plane separates the cavity into two cells, each of which has 40 ferrite rings and a single-ended ceramic accelerating gap. The cavity is in air and only the beam pipe is under vacuum. Each ferrite ring is 0.0254 m thick and has inner/outer radii of 0.125/0.25 m. Based on measurements in [11], it appears that a safe operating field of 0.0049 T is possible at 6 MHz without thermal runaway problems. This means that each ring can generate 583 volts and each cavity can generate 23.5 kV/cell and 47 kV/cavity. A 3-mm-thick cooling plate is clamped between ferrite rings. The ferrite rings are mounted together in groups of 20 and a figure-8 bias winding is wound around two groups of 20 ferrites per cell to provide dc excitation with rf cancellation at the input.

The two cells are connected together by a rigid coaxial line that is directly connected to the ceramic gaps. A single amplifier tube excites the two gaps in parallel as is done on the ISIS RCS. A total of 43 cavities are needed to provide the required peak accelerating voltage of 2MV per turn. The cathode-follower amplifier is planned to compensate for and control beam loading problems. It is expected that feed-forward will be needed to handle the initial shock caused by the one-turn injection from the 2-GeV ring.

VIII.5 Control System

The control system design is similar to that planned for the 1-MW source, described in [1]. High-performance workstations act as operator consoles, distributed microprocessors control the equipment interfacing and preprocess data, and a network connects the system together. The control system is a direct application of EPICS, the Experimental Physics and Industrial Control System, described in [12] and the references therein.

VIII.6 Beam Diagnostic Instrumentation – RCS-II and Transport Lines

Diagnostic instrumentation is used to monitor beam position, profile, current, and beam losses in RCS-II and in its associated transport lines. The types of beam diagnostics provided for RCS-II and the transport lines include beam position monitors, current monitors, and loss monitors. Specialized diagnostic instrumentation, such as moving wire scanners and Faraday cups, is provided for beam studies. Interlocked target protection secondary emission monitors are also provided.

IX. Summary

A feasibility study for a pulsed spallation source based on a 5-MW, 10-GeV rapid cycling proton synchrotron (RCS) is in progress. The 10-GeV synchrotron uses as its injector the 2-GeV accelerator system from a 1-MW source [1-7]. The 1-MW source accelerator system consists of a 400-MeV proton linac with 2.5 MeV energy spread in the 75% chopped beam, and a 30-Hz RCS that accelerates the 400-MeV beam to 2 GeV. The 10-GeV RCS accepts and accelerates the 0.5 mA of beam at 2 GeV to 10 GeV. Beam transfer from the 2-GeV synchrotron to the 10-GeV machine utilizes highly efficient bunch-to-bucket injection, so that

the transfer can be made without beam loss. The synchrotron lattice uses FODO cells of 90° phase advance. Dispersion-free straight sections are obtained using a missing magnet scheme. The synchrotron magnets are powered by a dual-frequency resonant circuit. The magnets are excited at a 20-Hz rate and de-excited at 60-Hz, resulting in an effective 30-Hz rate. A key feature of the design of this accelerator system is that beam losses are minimized from injection to extraction, reducing activation to levels consistent with hands-on maintenance. The low losses are achieved by providing large dynamic aperture in the transverse plane and sufficient bucket area in the longitudinal plane.

X. References

[1]   "IPNS Upgrade - A Feasibility Study", ANL Report ANL-95/13 (April, 1995).
[2]   E. Lessner, Y.-C. Chae, and S. Kim, "Effects of Imperfections on Dynamic Aperture and Orbit Functions of the IPNS Upgrade Synchrotron," Proc. of the 1995 Particle Accelerator Conference, Dallas, Texas, May 1995, to be published.
[3]   Y.-C. Chae and Y. Cho, "Study of Field Ionization in Charge Exchange Injection for the IPNS Upgrade," Proc. of the 1995 Particle Accelerator Conference, Dallas, Texas, May 1995, to be published.
[4]   E. Crosbie and K. Symon, "Injecting a Kapchinskij-Vladimirskij Distribution into a Proton Synchrotron," Proc. of the 1995 Particle Accelerator Conference, Dallas, Texas, May 1995, to be published.
[5]   K. Harkay, Y. Cho, and E. Lessner, "Longitudinal Instability Analysis for the IPNS Upgrade," Proc. of the 1995 Particle Accelerator Conference, Dallas, Texas, May 1995, to be published.
[6]   K. Harkay and Y. Cho, "Transverse Instabilities Analysis for the IPNS Upgrade," Proc. of the 1995 Particle Accelerator Conference, Dallas, Texas, May 1995, to be published.
[7]   Y. Cho, et al., "Feasibility Study of a 1-MW Pulsed Spallation Source," these proceedings.
[8]   Y. Cho, E. Lessner, and K. Symon, "Injection and Capture Simulations for a High Intensity Proton Synchrotron," Proc. of the European Particle Accelerator Conference, page 1228 (1994).
[9]   G. H. Rees, "Status Report on ISIS," Proc. of the IEEE Particle Accelerator Conference (March 16-19, 1987).
[10]   G. H. Rees, "Status of the SNS," IEEE Transactions on Nuclear Science, Vol. NS-30, No. 4, August 1983.
[11]   M. A. Goldman, et al., "Studies Of Ferrite Materials For The AGS Booster Synchrotron", Proc. of the IEEE Accelerator Conference, Chicago, IL, March 20-23, 1989.
[12]   McDowell, et al., "Status of the Advanced Photon Source and its Accelerator Control System," Nucl. Instrum. and Methods A 352 13 (1994).

DISCLAIMER